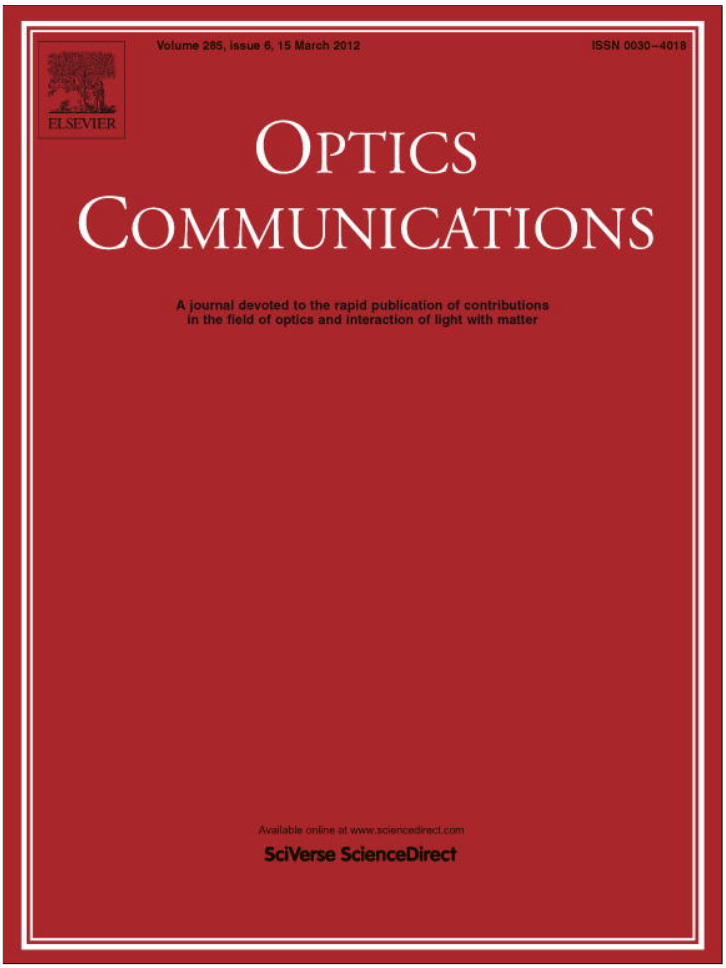

Optics Communications 285 (2012) 1519–1522

Contents lists available at SciVerse ScienceDirect

Optics Communications

journal homepage: www.elsevier.com/locate/optcom

Subwavelength beam focusing by multiple-metal slits surrounded by chirped dielectric surface gratings

Sen Jia, Lihe Yan, Jinhai Si *, Wenhui Yi, Feng Chen, Xun Hou

Key Laboratory for Physical Electronics and Devices of the Ministry of Education & Shaanxi Key Lab of Information Photonic Technique, School of Electronics & information Engineering, Xi'an Jiaotong University, Xianning-xilu 28, Xi'an, 710049, China

ARTICLE INFO

Article history:
Received 15 August 2011
Received in revised form 24 September 2011
Accepted 15 November 2011
Available online 28 November 2011

Keywords:
Surface plasmon polaritons
Subwavelength
Beam focusing
Metal slit

ABSTRACT

A novel method is proposed to actualize the beam focusing through multiple subwavelength metal slits surrounded by chirped dielectric surface gratings. The slits have equal widths, depths, and interspaces. The electro-magnetic energy is transported by the slits in the form of surface plasmon polaritons (SPPs). The dielectric gratings converge surface plasmon wave on a single point. Numerical simulation of the design example is performed through finite-difference time-domain (FDTD) method. The results show that the focal length is just several times of the incident wavelength and the cross section of focus spot is far narrower than the incident wavelength.

1. Introduction

In recent years, the metallic subwavelength structures have caused great interests of people due to the discovery of extraordinary optical transmission phenomena through subwavelength metallic aperture array [1–3]. Lezec et al. firstly observed that the light emerging from a nano aperture surrounded by periodic corrugation on the exit side of a metallic thin film displays highly directed beaming with a low divergence [4]. Simulations and experiments validate that the surface plasmon polaritons (SPPs), resonantly excited in the corrugated metallic surface are accountable for these phenomena [1–8]. This opens up new areas of research for various subwavelength-optics devices with thin metallic films. Many plasmonic devices based on thin metallic film with slit have been proposed such as filter, all optical switch, interferometer, waveguide, etc. [9–18]. Among these, the devices which are capable of converging light are noticed especially by researchers. Many excellent works about metallic nanolens have been reported [16–22]. Some metal structures such as a curved slit flanked with concentric periodic grooves [20], nanoholes arrays [21], and a central slit surrounded by the grooves [22] have been experimentally demonstrated capable of converging SPPs. Besides, Sun and Kim have designed a metallic nanolens with slits perforated on a thin metallic film [16], which brings different phase retardations to the light transmitted through them for variant slit depths. Shi has designed a metallic nanolens based on slits array with equal depths and variant widths perforated on a thin metallic film [17]. Furthermore, Kim proposed a method for optical beam focusing by a single subwavelength metal slit surrounded by chirped surface gratings [18]. The device requires at least six dielectric gratings on each side of a single metal slit to perform the beam focusing. The full width at half maximum of the focus spot is a little narrower than the incident wavelength. Thus, to further improve the resolution of the plasmonic lens composed of metal slit and dielectric grating is desired to achieve objective.

In this letter, we propose a design for focusing the beam by employing multiple subwavelength metal slits surrounded by chirped dielectric surface gratings. The metal slits have equal widths, depths, and interspaces. The chirped dielectric surface gratings result in the difference of phase retardation of SPPs from metal slits, which is utilized to perform subwavelength beam focusing. Simulation results show the focal length can be controlled and changed in the range of the order of wavelength by adjusting the gratings parameter and the cross section of focus spot is far narrower than the incident wavelength.

2. Principle

The schematic diagram of our proposed beam focusing structure is shown in Fig. 1(a). Multiple subwavelength metal slits are surrounded by chirped dielectric surface gratings. The slits have equal widths, depths, and interspaces. The incident field is the p-polarized monochromatic wave (TM wave). The SPPs are excited from the metal slit and they propagate along each side on the metal silt in the form of a waveguide mode for polarized case. When the SPPs are propagating on the corrugated surface, the radiation field can be generated from the surface gratings. In previous reports, different phase retardations can be achieved when the light is transmitted through metal slits with variant depths [16] or widths [17], which

* Corresponding author.
E-mail address: jinhaisi@mail.xjtu.edu.cn (J. Si).

0030-4018/$ – see front matter.
doi:10.1016/j.optcom.2011.11.040

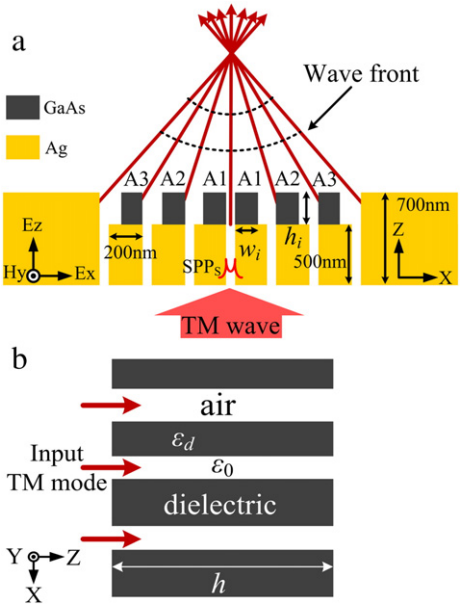

Fig. 1. The schematic diagram of the introduced beam focusing structure. (a) Seven subwavelengths surrounded by dielectric surface gratings on the output metal surface. A TM-polarized plane wave (consists of Ex, Hy and Ez field component, and Hy component parallel to the *y*-axis) is incident to the slit array from the bottom side. (b) Dielectric waveguide array.

can be utilized to implement beam focusing. In other words, a large depth or width can all result in large phase retardation. In our structure, however, due to the slits with equal width and depth, the difference of phase retardations between slits is zero when the SPPs are propagating at metal slits zone. However, the position is quite different at dielectric gratings zone. Considering two closely placed surface gratings as a plane dielectric waveguide with air core and finite length of h, then the surface gratings can be considered as a dielectric waveguide array. That is so-called slot waveguide array.

The schematic diagram of the waveguide array is shown in Fig. 1(b). Here, we select a dielectric with high refractive index as the gratings, or in other words the wall of waveguide. Because of the large index contrast between core and wall in the structure, it produces a high degree of optical confinement in the air core that is very similar to the hollow metallic waveguide [23]. The principle of the dielectric waveguide is based on the discontinuity of the normal component of the electric field at the high index-contrast interface. The component of the electric field (Ex) of the TM wave is perpendicular to high-index regions, undergoing strong discontinuity at the high index-contrast interface, with much higher amplitude in the low-index regions (air core). The ability of confining light in the structure is also experimentally demonstrated in nanometer-size slot waveguide [24]. The phase of SPPs waveguide mode transmitted through the dielectric waveguide can be expressed as

$$\phi_{\text{total}} = \phi_{\text{metal}} + \Delta\phi + \beta h - \theta \tag{1}$$

Where ϕ_{metal} is the initial phase at the exit interface of metallic slit, the values of ϕ_{metal} from different slits are equal, θ the phase retardation induced by reflections between two adjacent gratings interfaces, $\Delta\phi$ is the accompanied phase changes at the exit interface of dielectric waveguide, β the propagation constants in dielectric waveguide, and βh is the phase retardation of SPPs mode propagation in dielectric waveguide. Both physical analysis and numerical simulation show that the product βh plays a dominating role when SPPs mode transmitted through metal slit with finite length of h [17]. Considering the similar characteristic in high optical confinement between the dielectric waveguide and metallic slit, the conclusion also comes into existence in the dielectric waveguide. The propagation constants β of SPPs mode in the dielectric waveguide can be calculated by solving the equation [25]

$$\tan\left(H\sqrt{k_0^2 n_H^2 - \beta^2} - \theta\right) = \frac{n_H^2}{n_S^2}\frac{\sqrt{\beta^2 - k_0^2 n_S^2}}{\sqrt{k_0^2 n_H^2 - \beta^2}} \tanh\left(\frac{w}{2}\sqrt{\beta^2 - k_0^2 n_S^2}\right) \tag{2}$$

$$\theta = \arctan\left(\frac{n_H^2}{n_C^2}\frac{\sqrt{\beta^2 - k_0^2 n_C^2}}{\sqrt{k_0^2 n_H^2 - \beta^2}}\right) \tag{3}$$

where k_0 is the wave vector of light in free space; n_S, n_C and n_H stand for the indices of air core, air cladding, and dielectric, respectively. Due to the core and cladding of dielectric waveguide are air, the indices of them are same. H and w are the widths of the dielectric grating and air core, respectively. Because of the chirp of surface gratings, the distance between two adjacent gratings is changed. This means the air cores of the plane dielectric waveguides have different widths.

Fig. 2 gives the calculated results of propagation constant β versus air core width w and dielectric grating width H. GaAs is chosen as the material of the dielectric gratings because of its high refractive index [26]. The refractive index of GaAs is 3.664 at 800 nm [27]. The refractive index of air is 1. From the figure, we note that the effective index $\text{Re}(\beta/k_0)$ of the slot waveguide is decreased with increasing width of the air core. Therefore, the phase retardation introduced by central gratings is larger than that introduced by the gratings on both sides. This character is utilized to perform beam focusing.

3. Design and simulation

Two-dimensional finite difference time domain (FDTD) simulation is performed to demonstrate the validity of the structure. Simulation region is surrounded by the perfect matched layer (PML) absorber. In the FDTD algorithm, the grid sizes in the x and the z directions are chosen to be 5 nm × 5 nm. The wavelength of incident TM polarized light is 800 nm in air. The metal assumed is silver. The frequency-dependent complex relative permittivity of silver is characterized by the Drude model

$$\varepsilon_m(\omega) = \varepsilon_\infty - \frac{\omega_p^2}{\omega(\omega + i\gamma)} \tag{4}$$

Here $\omega_p = 1.38 \times 10^{16}$ Hz is the bulk plasma frequency, which represents the natural frequency of the oscillations of free conduction

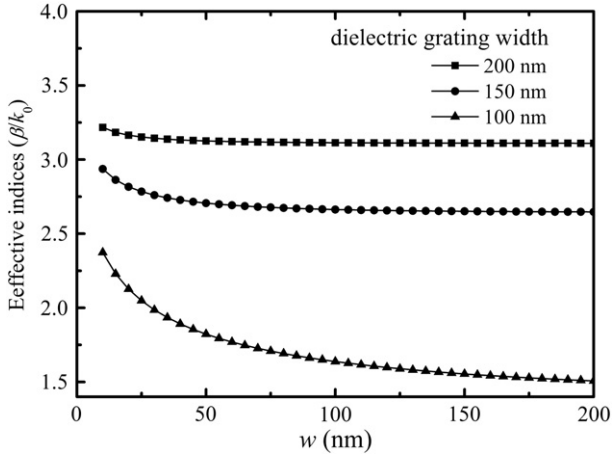

Fig. 2. The calculated results of propagation constant β versus air core width w and dielectric grating width H at a wavelength of 800 nm.

electrons; $\gamma = 2.73 \times 10^{13}$ Hz is the damping frequency of the oscillations, ω is the angular frequency of the incident electromagnetic radiation, and ε_∞ stands for the dielectric constant at infinite angular frequency with a value of 3.7 [28]. The silver film is composed of transparent and opaque zone. The thickness of opaque zone of silver film is 700 nm as shown in Fig. 1(a). The slits with equal width are formed in the transparent zone of silver film with 500-nm-thickness. The interspacing between adjacent slits is 250 nm (center to center) and slit width is 50 nm with slit depth of 500 nm, as a compromise of acceptable manufacture difficulty and optical quality. Slits are surrounded by dielectric surface gratings on the output metal surface. In design, the chirped dielectric gratings are fabricated on the strip of the metal film to avoid gratings damage. Moreover, this configuration will help to decrease device dimension. In order to simplify the fabrication, the outermost dielectric gratings are replaced by metallic corners.

4. Results and discussions

Fig. 3(a) shows FDTD simulation of time-average electric-field intensity distribution of beam focusing in the structure. The position of focus is indicated by horizontal white lines in z-axis. The height and width of the gratings are denoted with h_i, w_i and $i = 1, 2, 3$, respectively, as shown in Fig. 1(a). The surface gratings are fabricated on one side of interspacing, rather than in the center. The corresponding surface gratings parameters are $h_i = 200$ nm, $w_1 = 160$ nm, $w_2 = 145$ nm, and $w_3 = 135$ nm. The electric field intensity $|Ex|^2$ is used to represent the field intensity distribution. After 50,000 steps of calculation, the resulting intensity distribution of the radiated light is obtained and showed in Fig. 3(a). The exit side of metal surface is posited at $z = 0.5$ μm and cross section of the focus at $z = 1.655$ μm. A beam spot appears about 1.155 μm away from the exit metal surface. The cross section of focus spot in x direction is given in Fig. 3(b), indicating a full-width at half-maximum (FWHM) of 472 nm. The important point of simulation result shows that the focal length can be little larger than the wavelength and the cross section of focus spot can be far narrower than the incident wavelength.

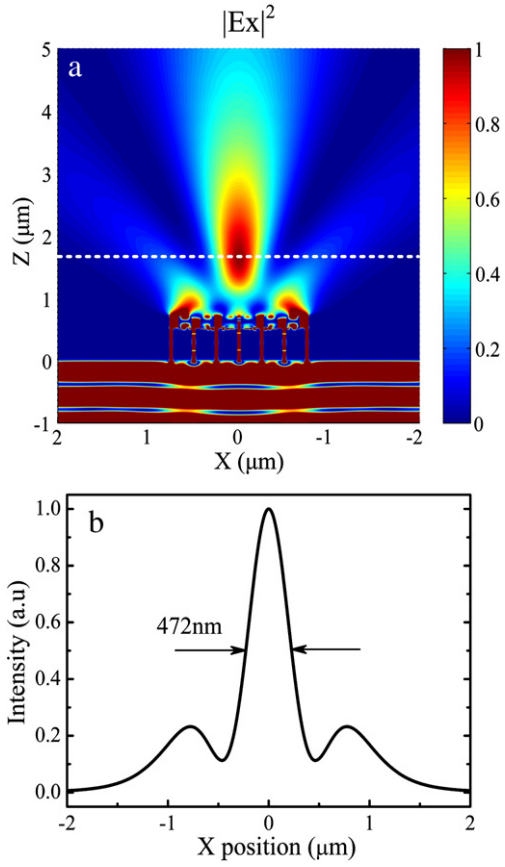

Fig. 3. (a) FDTD calculated results of the electric-field intensity $|Ex|^2$ time-average distribution for designed beam focusing structure. (b) Cross sections of the focus.

Fig. 4 shows the simulated transverse field distributions in metal slits and slot waveguides. The positions are located at $z = 0.6$ μm for air core and $z = 0.3$ μm for metal slits, respectively. In the figure, one can clearly see the strong field confinement in the slot waveguides. As a result, the lights from slits (excluding two outermost slits) cannot transport from slits to the two metallic corners and are reflected by them. Therefore, although the metallic corners can reflect a part of light from the two outermost slits toward the focus spot (shown in Fig. 3(a)), most of the light is manipulated by the dielectric gratings and converge toward the focal spot. This means the phase delay caused by the dielectric grating is the principal cause of forming a beam focus. Relatively good agreement is obtained between the technical analysis and the simulated results.

Due to the fact that the radiations of SPPs are generated from the surface gratings, the parameters of surface gratings directly influence the focusing performance of the structure. In order to understand the dependence of beam focusing on the highs of surface gratings well, the field intensity distributions for varied highs are drawn in Fig. 5 for comparison. Here, the widths of gratings are fixed and highs are decreasing gradually. The original high of surface gratings is set as $h_0 = 190$ nm, while the decreases of modulated gratings high can be defined as $h_N = -NL_{step} + h_0$, $N = 0,1,2,3,\ldots$, where h_N is the high of gratings. The step L_{step} is 10 nm.

From the figure, we note that the FWHMs increase from 472 nm to 671 nm with the decreasing gratings high. The corresponding focal lengths are changed from 1.145 μm to 1.33 μm. More details of the dependence of focal length and width on gratings high are shown in Fig. 5(e). Simulation results show clearly that the beam has a tendency to ultimately diverge when the highs are continuously decreased. It is noteworthy that the parameters of two metallic corners remain constant in the course of gratings high varying. Thus, their influence on the beam manipulating is also constant. This corroborates the fact that the surface gratings result in beam focusing rather than the metallic corners. Obviously, the decrease of high of the dielectric gratings can lead to the diminishing of the difference of phase retardations between dielectric waveguides. As a result, the beam tends to diverge.

As mentioned above, the advantage of the plasmonic lens proposed over a usual convex lens is its compact structure, which allows for easy integration in on-chip applications. Compared with the previous structures [16,19], our design has a smaller spot size, shorter

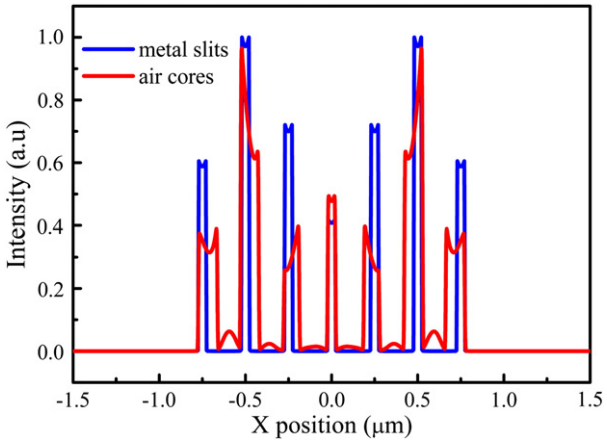

Fig. 4. The electric-field intensity $|Ex|^2$ time-average distribution in metal slits and air core of dielectric waveguides, respectively.

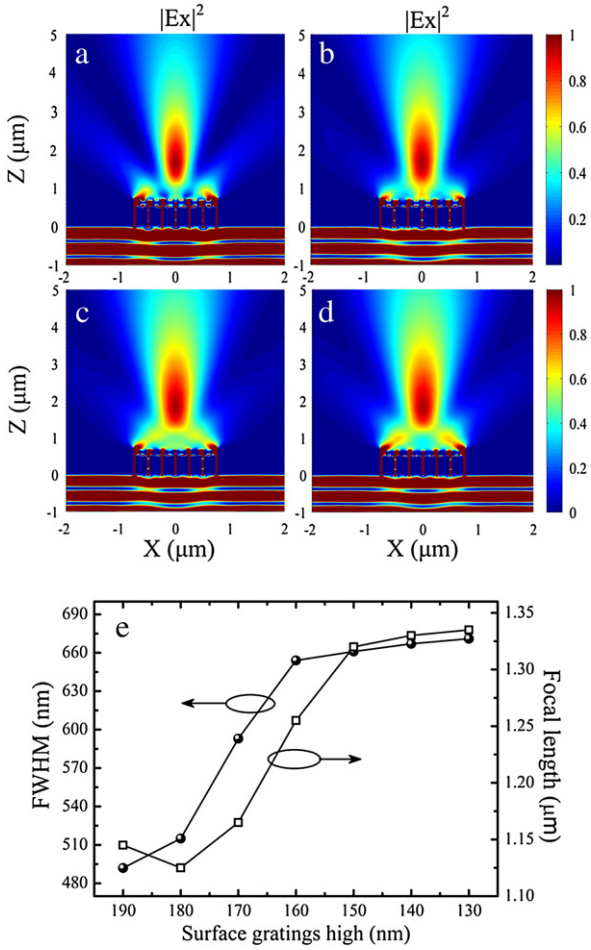

Fig. 5. Field distributions ($|Ex|^2$) of the beam focusing structure for different surface gratings highs: (a) $h_0=190$ nm, (b) $h_2=170$ nm, (c) $h_4=150$ nm, (d) $h_6=130$ nm. The widths of gratings are fixed and are the same as those used in Fig. 2(a). (e) The dependence of focal length and focal spot on the width of surface gratings.

working distance, and sampler configuration. After a plane wave passes through the 1.55 μm wide plasmonic lens, it is focused 1.155 μm above the lens, resulting in an NA of 0.56.

5. Conclusion

In summary, a beam focusing structure composed of multiple metal nano-slits surrounded by chirped dielectric surface gratings is introduced. The slits have equal widths, depths, and interspaces. Numerical simulation through FDTD shows that the structure can result in a clear focus spot with a size far narrower than the incident wavelength. The minimal focal spot with a 472 nm FWHM is obtained when incident wavelength is 800 nm. The focal length and focal spot size of the structure can be changed in the range of the order of wavelength by adjusting the surface gratings appropriately. These advantages promise this structure to find potential applications in integrate optics, date storage, and near-field imaging.

Acknowledgements

The authors gratefully acknowledge the financial support for this work provided by the National Basic Research Program of China (973 Program) under the Grant No. 2012CB921804, and the National Science Foundation of China under the Grant Nos. 91123028 and 11074197.

References

[1] H.F. Ghaemi, T. Thio, D.E. Grupp, T.W. Ebbesen, H.J. Lezec, Physical Review B 58 (1998) 6779.
[2] L.M. Moreno, F.J. Garcia-Vidal, H.J. Lezec, K.M. Pellerin, T. Thio, J.B. Pendry, T.W. Ebbesen, Physical Review Letters 86 (2001) 1114.
[3] T.W. Ebbesen, H.J. Lezec, H.F. Ghaemi, T. Thio, P.A. Wolff, Nature 391 (1998) 667.
[4] H.J. Lezec, A. Degiron, E. Devaux, R.A. Linke, F. Martin-Moreno, L.J. Garcia-Vidal, T.W. Ebbesen, Science 297 (2002) 220.
[5] L.M. Moreno, F.J. Garcia-Vidal, H.J. Lezec, A. Degiron, T.W. Ebbesen, Physical Review Letters 90 (2003) 167401.
[6] F.J. Garcia-Vidal, H.J. Lezec, T.W. Ebbesen, L.M. Moreno, Physical Review Letters 90 (2003) 213901.
[7] G. Veronis, S. Fan, Applied Physics Letters 87 (2005) 131102.
[8] T. Lee, S. Gray, Optics Express 13 (2005) 9652.
[9] J. Tao, X.G. Huang, X.S. Lin, Q. Zhang, X.P. Jin, Optics Express 17 (2009) 13989.
[10] J. Tao, X.G. Huang, S.H. Liu, Journal of the Optical Society of America B 27 (2010) 1430.
[11] L. Wang, S.M. Uppuluri, E.X. Jin, X.F. Xu, Nano Letters 6 (2006) 361.
[12] J.L. Liu, H.F. Zhao, Y. Zhang, S.T. Liu, Applied Physics B 98 (2010) 797.
[13] S. Passinger, A. Seidel, C. Ohrt, C. Reinhardt, A. Stepanov, R. Kiyan, B. Chichkov, Optics Express 16 (2008) 14369.
[14] Z. Han, L. Liu, E. Forsberg, Optics Communications 259 (2006) 690.
[15] S.I. Bozhevolnyi, V.S. Volkov, E. Devaux, J.Y. Laluet, T.W. Ebbesen, Nature 440 (2006) 508.
[16] Z.J. Sun, H.K. Kim, Applied Physics Letters 85 (2004) 642.
[17] H.F. Shi, C.T. Wang, C.L. Du, X.G. Luo, X.C. Dong, H.T. Gao, Optics Express 13 (2005) 6815.
[18] S. Kim, Y. Lim, H. Kim, J. Park, B. Lee, Applied Physics Letters 92 (2008) 013103.
[19] F. Hao, R. Wang, J. Wang, Plasmonics 5 (2010) 45.
[20] F. Lopez-Tejeira, Sergio G. Rodrigo, L. Martin-Moreno, F.J. Garcia-Vidal, E. Devaux, T.W. Ebbesen, J.R. Krenn, P. Radko, S.I. Bozhevolnyi, M.U. Gonzalez, J.C. Weeber, A. Dereux, Nature Physics 3 (2007) 324.
[21] L. Yin, V.K. Vlasko-Vlasov, J. Pearson, J.M. Hiller, J. Hua, U. Welp, D.E. Brown, C.W. Kimball, Nano Letters 5 (2005) 1399.
[22] F.H. Hao, R. Wang, J. Wang, Optics Express 18 (2005) 15741.
[23] M.H. Ibanescu, S.G. Johnson, M. Soljačić, J.D. Joannopoulos, Y. Fink, Physical Review E 67 (2003) 046608.
[24] Q.F. Xu, V.R. Almeida, R.R. Panepucci, M. Lipson, Optics Letters 29 (2004) 1626.
[25] V.R. Almeida, Q.F. Xu, C.A. Barrios, M. Lipson, Optics Letters 29 (2004) 1209.
[26] P. Jouy, Y. Todorov, A. Vasanelli, R. Colombelli, I. Sagnes, C. Sirtori, Applied Physics Letters 98 (2011) 021105.
[27] S. Zollner, Journal of Applied Physics 90 (2001) 515.
[28] X.S. Lin, X.G. Huang, Optics Letters 33 (2008) 2874.